JOURNAL OF MECHANICS OF CONTINUA AND MATHEMATICAL SCIENCES
www.journalimcms.org

ISSN (Online) : 2454 -7190 , Special Issue, No.-12, August (2025) pp 80-93 ISSN (Print) 0973-8975

MATHEMATICAL MODELING OF SINTER FORGING DYNAMICS CONSIDERING DIFFERENT ASPECT RATIO AND FRICTIONAL CONDITION

Navdeep[1], Parveen Kumar[2], R. K. Ranjan[3], K. D. Sharma[4]

[1,2] Department of Mathematics, J. C. Bose University of Science and Technology, Sector-6, Faridabad, Haryana, 121006, India.

[3] Department of Mechanical Engineering, Government Polytechnic, Vidya Peeth Chowk, Lakhisarai, Bihar, 811311, India.

[4] Department of Mathematics, Chitkara University Institute of Engineering and Technology, Punjab, 140401, India.

Corresponding author: **Parveen Kumar**

Email: [1]navdeepvar394@gmail.com, [2] parveengaur1980@gmail.com
[3] rkranjanbit@gmail.com, [4] krishandutt.sharma@chitkara.edu.in

https://doi.org/10.26782/jmcms.spl.12/2025.08.00007

(Received: May 16, 2025; Revised: July 26, 2025; Accepted: August 09, 2025)

Abstract

The proposed model addresses the limitations of existing analytical methods, such as equilibrium and lower-bound approaches, by considering height reduction, relative density increments, and varying die-workpiece interactions simultaneously. The model's predictions align closely with experimental results, demonstrating its reliability and accuracy. This research paves the way for the development of industrial-grade software tools, offering manufacturers a competitive edge by improving process predictability and reducing dependence on computationally intensive methods like the Finite Element Approach.

Keywords: Sinter Forging, Analytical Modeling, Upper Bound Dynamics, Aspect ratio.

I. Introduction

Sinter forging is a manufacturing process used to produce components from metal powders by forging pre-sintered metal-powder preforms. This process simultaneously achieves compaction and densification of the material. Sinter forging has emerged as a rapidly advancing net-shape manufacturing technology, enabling the mass production of high-performance and precise engineering components at competitive costs while minimizing scrap loss. By integrating the benefits of powder metallurgy and conventional forging, this process ensures a robust metallurgical structure through powder compaction,

eliminates energy-intensive operations, and imparts desirable mechanical properties through forging. The products resulting from sinter forging exhibit mechanical and metallurgical properties comparable to wrought metals [IX, XIII].

For the past 50 years, sinter forging has been a significant area of active research with the primary aim of achieving industrial-level application to reduce energy consumption and scrap while utilizing resources efficiently. Researchers have explored the impact of various factors such as friction and adhesion, both of which are influenced by applied pressure during the manufacturing process [VIII, XVII]. The coefficient of friction, for instance, plays a crucial role in determining the required load, and it increases significantly in the absence of lubrication [XVIII].

Unlike conventional forging of wrought metals, sinter forging must address the characteristic porous nature of materials during compression. The process introduces a unique deformation pattern influenced by factors such as the relative density of the preform and the die-workpiece interface. Notably, the deformation of sintered metals differs significantly at high speeds compared to slow speeds due to variations in flow stress [I, VI, VII]. The effect of speed remains a critical aspect in the forging of sintered metals [XIV, XV, XVI]. Intrinsic parameters such as the density-dependent friction term, strain hardening, and material constants generally differ for different materials. These have different densities of atoms, distinct crystal structures, and interatomic forces.

Over the years, researchers have attempted to model sinter forging analytically using various mathematical approaches, including equilibrium and lower-bound methods. However, no existing model has fully captured the complexity of the process due to the dynamic interplay of numerous factors. These include height reduction, density increment, flow stress variation, changing friction, increasing powder density, billet width expansion, and Poisson's ratio effects. Our proposed model incorporates all these factors in a realistic manner for open die forging, making it highly applicable for industrial use. The paper aims to highlight the requirement of realistic analytical modeling considering all the dynamic factors.

II. Mathematical Modeling

II.i. Improved Friction

The coefficient of friction (μ) depends on the lubrication material and the preform's relative density$\mu = 10 \cdot \mu_0 \cdot (\rho_i)^{\epsilon}$.

The sticking radius $r_{m_{i+1}} = b_i \cdot (1 - (1 - \rho_i)^{\mu})$

II.ii. Dynamics of Sinter-Forging

Early research often overlooked evolving factors during the sinter-forging of sintered preforms. In this process, relative density increasesleading to changes in flow stress, friction, and powder density with percentage height reduction. The calculations are based on cylindrical geometry. For other shapes, adjustments may be required. The process is in

an infinitesimal step size.

The final density $\rho_f = \frac{\rho_i}{\left(1+\nu\frac{\Delta h}{h}\right)^2\left(1-\frac{\Delta h}{h}\right)}$

The incremental height reduction (Δh_{i+1}) and the current height (h_i)

$$\Delta h_{i+1} = h_0\left(\frac{\text{height reduction percent}_{i+1} - \text{height reduction percent}_i}{100}\right)$$

$$h_i = h_0\left(1 - \frac{\text{height reduction percent}}{100}\right)$$

The density evolution $\rho_{i+1} = \frac{\rho_i}{\left(1+\nu_i\frac{\Delta h_i}{h_0}\right)^2\left(1-\frac{\Delta h_i}{h_0}\right)}$

The width at any stage $b = b_0\left(1+\nu\frac{\Delta h}{h}\right)$; $b_{i+1} = b_0\left(1+\nu_i\frac{\Delta h_i}{h_0}\right)$

Poisson's ratio at each step $\nu_{i+1} = 0.5 \times {\rho_i}^{1.92}$ or equivalently $\nu_{i+1} = \frac{\frac{\Delta b_i}{b_i}}{\frac{\Delta h_i}{h_i}}$

The flow stress evolves $\lambda_{i+1} = \frac{\rho_i^k \cdot \sigma_0}{1-2\cdot\eta_i}$ Finally, powder density $\rho_{p_{i+1}} = \rho_s \cdot \rho_i$

II.iii. Velocity Field

$$U_r = \nu\frac{U}{h}r \quad (1)$$

$$U_z = -z\frac{U}{h} \quad (2)$$

$$U_\theta = 0 \quad (3)$$

satisfy the compatability equation[17] $\frac{\partial U_r}{\partial r} + \nu\frac{\partial U_z}{\partial z} = 0$ (4)

II.iv. Strain Rates

$$\dot{\varepsilon}_{rr} = \frac{\partial U_r}{\partial r} = \nu\frac{U}{h} \quad ; \quad \dot{\varepsilon}_{\theta\theta} = \frac{U_r}{r} = \nu\frac{U}{h} \quad ; \quad \dot{\varepsilon}_{zz} = \frac{\partial U_z}{\partial z} = -\frac{U}{h}$$

$$\dot{\varepsilon}_{r\theta} = \frac{1}{2}\left(\frac{\partial U_\theta}{\partial r} + \frac{1}{r}\frac{\partial U_r}{\partial \theta}\right) = 0 \quad ; \quad \dot{\varepsilon}_{rz} = \frac{1}{2}\left(\frac{\partial U_r}{\partial z} + \frac{\partial U_z}{\partial r}\right) = 0$$

$$\dot{\varepsilon}_{\theta z} = \frac{1}{2}\left(\frac{\partial U_z}{\partial \theta} + \frac{\partial U_\theta}{\partial z}\right) = 0 \quad ; \quad \dot{\varepsilon}_{rr} = \dot{\varepsilon}_{\theta\theta}$$

II.v. Upper bound

For plastic deformation, external power J^* [10-11]

$$J^* = W_i + W_f + W_a = PU \quad ; \quad J^* = \frac{2\sigma_0}{\sqrt{3}}\int_v \sqrt{\frac{1}{2}\dot{\varepsilon}_{ij}\dot{\varepsilon}_{ij}}\,\mathrm{d}v + \int_s \tau|\Delta V|\,\mathrm{d}s + \int_v \rho_\mathrm{p} a_i U_i \mathrm{d}v$$

(Wi) denotes the rate of internal energy dissipation

(Wf) denotes the frictional shear energy losses

(*Wa*) denotes energy dissipation by inertia forces
(*Wt*) covers the power supplied by body tractions.
In this case, no external surface traction is stipulated. Therefore, *Wt* = 0.

Internal Energy Dissipation

$$W_i = \frac{2\lambda}{\sqrt{3}}\int_0^h \int_0^b \sqrt{\frac{1}{2}\left(\dot{\varepsilon}_{rr}^2 + \dot{\varepsilon}_{\theta\theta}^2 + \dot{\varepsilon}_{zz}^2\right)}.2\pi r dr dz \quad \text{so } W_i = \sqrt{\frac{2}{3}}\pi\lambda U b^2\sqrt{1+2\nu^2}$$

Shear Frictional Energy Dissipation

$$W_f = \int_0^b \mu\left[p + \rho_0\phi_0\left\{1 - \left(\frac{r_{\mathrm{m}} - r}{nb}\right)\right\}\right](|U_r|_{z=0} + |U_r|_{z=h}).2\pi r dr$$

For practicality, consider $p = p_{av}$, where $p_{av} = \dfrac{P}{\pi b^2}$

$$W_{\mathrm{f}} = \frac{4\pi U\nu\mu p_{av} b^3}{h}\left[\frac{1}{3} + x\left\{\frac{1}{3}\left(1 - \frac{r_m}{nb}\right) + \frac{1}{4n}\right\}\right]$$

Inertial Energy Dissipation

$$W_{\mathrm{a}} = \int_0^b \int_0^h \rho_{\mathrm{p}}(a_r U_r + a_z U_z)2\pi r \,\mathrm{d}r\,\mathrm{d}z$$

Where $a_r = U_r\frac{\partial U_r}{\partial r} + U_z\frac{\partial U_r}{\partial z} + \frac{\partial U_r}{\partial t}$ $a_z = U_z\frac{\partial U_z}{\partial z} + \frac{\partial U_z}{\partial t}$

$$a_z = \frac{z}{h}\left(\frac{U^2}{h} - \dot{U}\right), a_r = \left(\nu\frac{r}{h}\right)\left[\nu\frac{U^2}{h} + \dot{U}\right] \text{ so } W_a = \pi\rho_p U b^2\left[\left(\nu\frac{U^2}{h} + \dot{U}\right)\nu\frac{b^2}{2} - \frac{U^2 - \dot{U}h}{3}\right]$$

Inertial energy dissipation[7], the parameters for aluminium preform:

$\mu_0 = 0.1$, $b = 11.5 \times 10^{-3}\mathrm{m}$, $h_0 = 18.9 \times 10^{-3}\mathrm{m}$, $n = 2.0$, $\rho_p = 2473.258\mathrm{kg/m^3}$, $U = 0.000025\mathrm{m/s}$, $\dot{U} = 0\mathrm{m/s^2}$, $x = 0.1$, $\rho_s = 2700\mathrm{kg/m^3}$.
By using the upper bound approach for open die plastic deformation

$$P = \frac{\sqrt{\frac{2}{3}}\pi\lambda b^2\sqrt{1+2\nu^2} + \pi\rho_p b^2\left[\left(\nu\frac{U^2}{h} + \dot{U}\right)\nu\frac{b^2}{2} - \frac{U^2 - \dot{U}h}{3}\right]}{1 - \frac{4\nu\mu b}{h}\left(\frac{1}{3} + x\left\{\frac{1}{3}\left(1 - \frac{r_m}{nb}\right) + \frac{1}{4n}\right\}\right)} \qquad (5)$$

III. Results and Discussion

By Figure 1. (a), for an initial low-density iron billet, the prediction of pressure is much closer to experimental values when the entire dynamics are considered. The percentage error is displayed above the experimental data at the corresponding % height reduction, as illustrated in the figure. The predictions of pressure are much closer to experimental values for aluminum sintered billet when the entire dynamics are considered, Figure 1. (b). This highlights the success of the modeling approach and its potential applicability in industrial use. For very high relative density preforms, the upper bound method acts as a reliable upper bound for pressure estimation, Figure 1. (c).

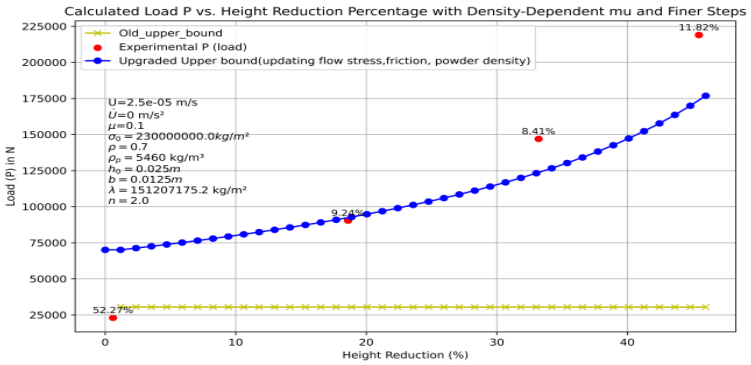

Fig. 1. (a) Variation of P w.r.t % height reduction for low ρpreform

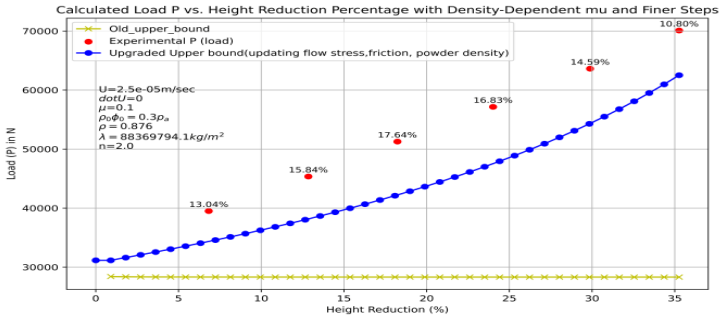

(b) Variation of P w.r.t. % height reduction for medium ρ preform

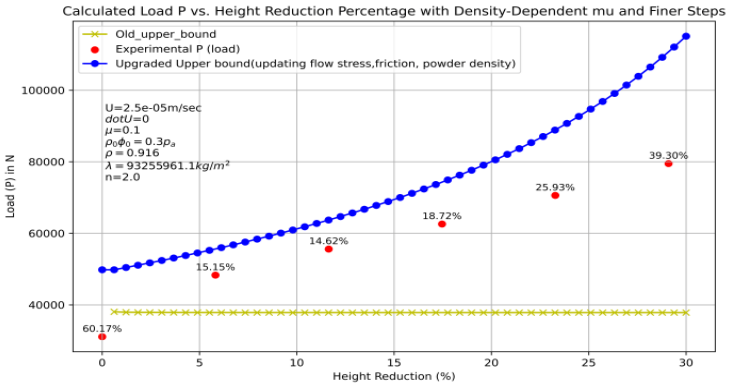

c) Variation of P w.r.t % height reduction for high ρ preform

Figure 1: Validation of P w.r.t. % height reduction for different ρ preform

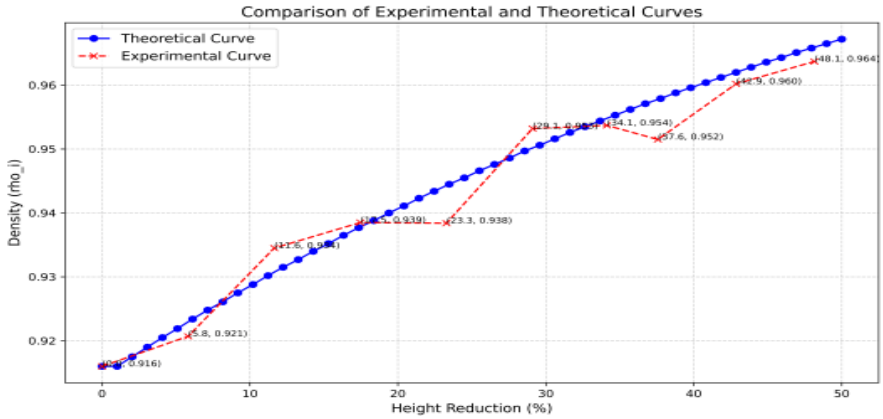

Fig. 2. Density variation with % height reduction

As shown in Figure 2, the modeling of densification closely aligns with the experimental curve by incorporating all the dynamic characteristics, including height reduction, billet expansion, increasing sticking radius, and friction. The theoretical data is in close agreement with experimental data from [4].

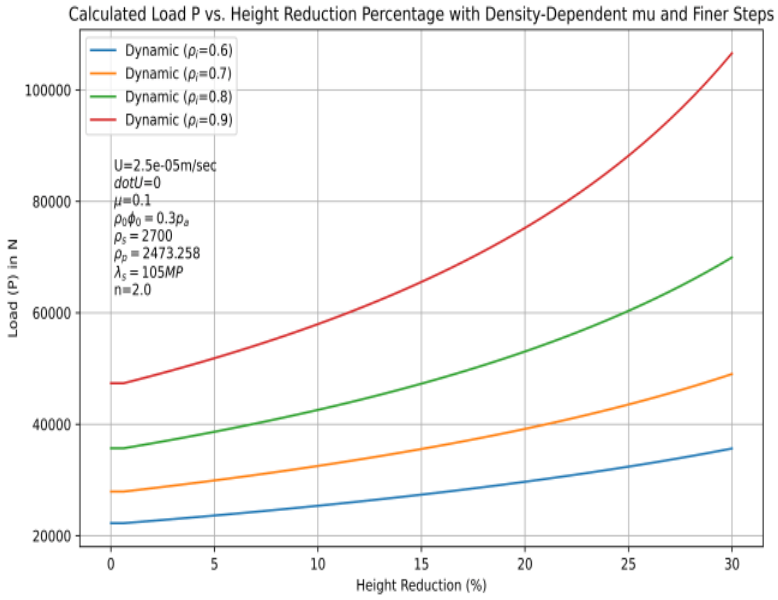

Fig. 3.

Fig. 3. P w.r.t % height reduction for different ρ preform of same aspect ratio

By Figure 3, pressure increases more sharply for high relative density greater than 0.8 and percentage height reduction greater than 5%.

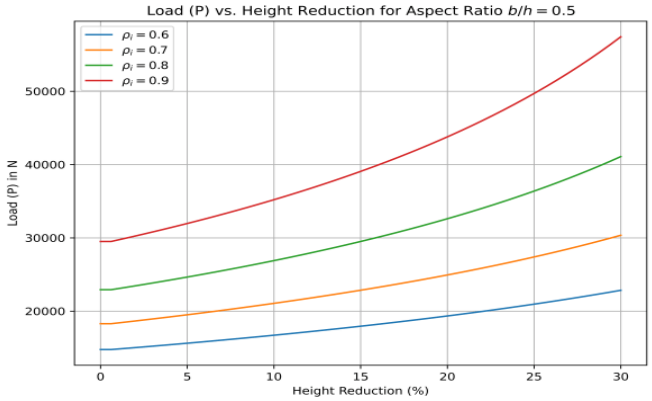

Fig. 4. (a) Pressure curve for Aspect Ratio = 0.5 for different ρ

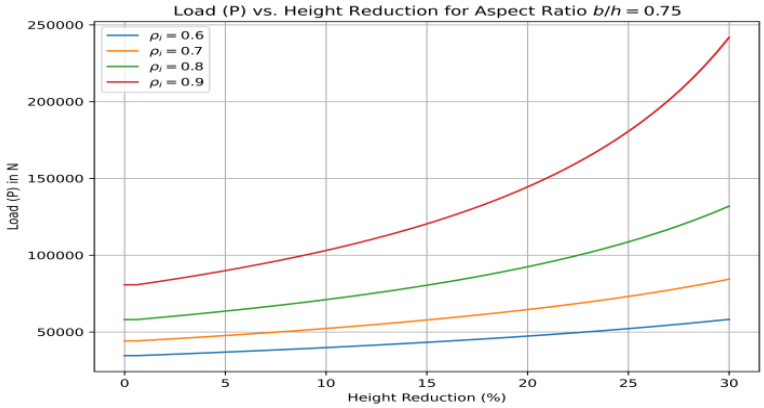

b. Pressure curve for Aspect Ratio = 0.75 for different ρ

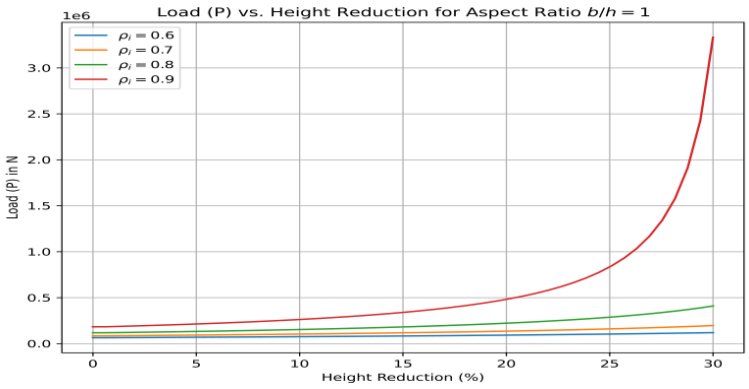

c. Pressure curve for Aspect Ratio = 1 for different ρ

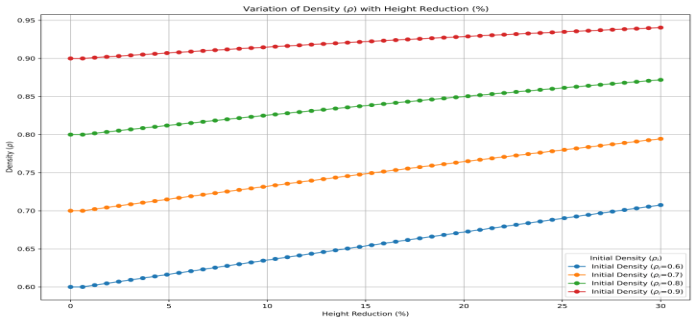

Fig. 5. Pressure curve for different aspect ratios for different ρ

For aspect ratio figures, the initial height is considered as $h_0 = 18.9 \times 10^{-3}$m. Width of the aluminum preform is chosen accordingly to maintain the specified aspect ratio.

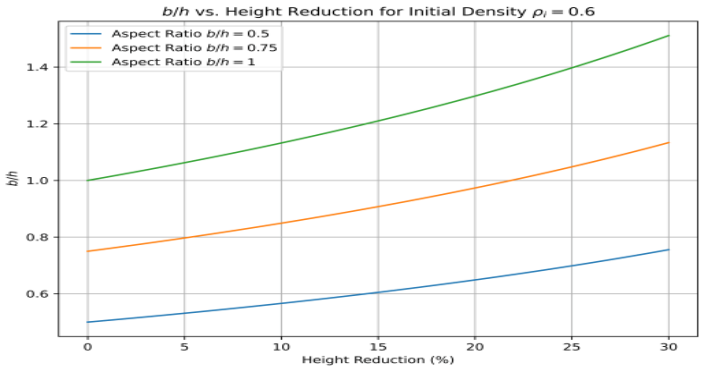

Fig. 6. (a) Aspect Ratio variation with % height reduction for $\rho = 0.6$

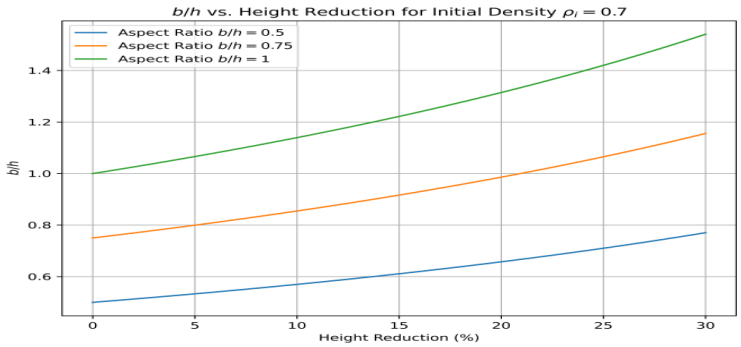

b. Aspect Ratio variation with % height reduction for $\rho = 0.7$

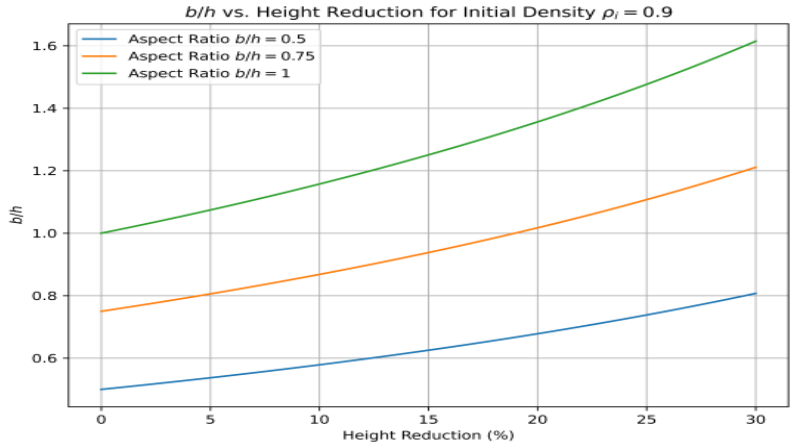

c. Aspect Ratio variation with % height reduction for $\rho = 0.8$

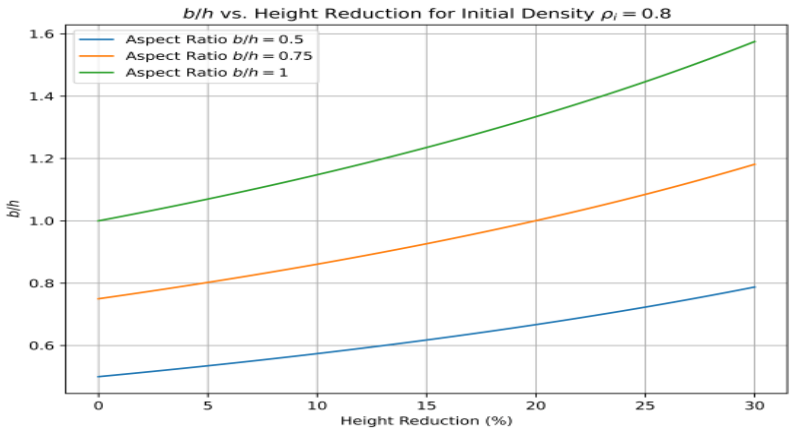

d. Aspect Ratio variation with % height reduction for $\rho = 0.9$

Figure 6: Aspect Ratio variation with % height reduction for different ρ values

Furthermore, as evident from Figures 6(a) to 6(d), low-aspect-ratio preforms show minimal variation in aspect ratio compared to high-aspect-ratio preforms. This behavior also depends on the relative density of the preform. Preforms with higher relative density exhibit greater variation in aspect ratio compared to those with lower density. This observation reflects a characteristic feature of sinter forging, where compaction progresses rapidly in the early stages. Subsequently, as densification approaches a critical threshold, the preform begins to behave more like wrought metal, leading to a shift in the compaction dynamics.

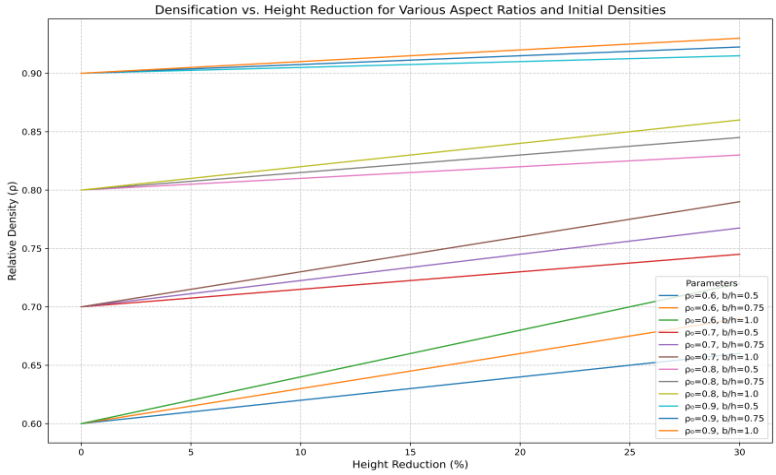

Fig. 7. Densification of different aspect ratio billets of different ρ

By Figure 7, it can be observed that low-density billets achieve densification at a faster rate with increasing percentage height reduction compared to high-density preforms. This is because low-density billets have more porosity to compact initially, allowing rapid densification in the early stages. Furthermore, high-aspect-ratio billets densify more rapidly than low-aspect-ratio billets, as their geometry facilitates better material flow during deformation, enhancing compaction efficiency. Preparation of the specimen and density measurements as per [10]. Equation (5), using the upper bound approach for plastic deformation in the case of open die forging, clearly exhibits the dependency on various process parameters such as flow stress, friction, variation in density, and speed. Inertial energy is significant at high acceleration.

It is evident from the graphs that not all billets densify at the same rate. The aspect ratio and initial relative density play a significant role in determining the densification behavior of sintered billets. High-aspect-ratio billets and low-initial-density preforms exhibit faster densification due to their inherent geometrical and material characteristics.

IV. Industrial Applicability

The proposed modeling approach for predicting pressure and densification during sinter forging demonstrates significant industrial relevance. By incorporating dynamic characteristics such as height reduction, billet expansion, and frictional effects, the model provides a more accurate representation of the forging process.

• **Optimized Process Parameters:** The model enables manufacturers to fine-tune parameters such as aspect ratio, initial relative density, and friction coefficients to achieve desired densification levels efficiently.

• **Material Savings:** Accurate predictions help reduce material wastage by minimizing over-forging or under-forging, ensuring optimal utilization of resources.

• **Cost-Effectiveness:** The ability to predict and control forging outcomes reduces trial-and-error experimentation, saving both time and costs in industrial setups.

• **Scalability:** The approach can be adapted to different geometries, material properties, and operational conditions, making it suitable for various applications, including automotive, aerospace, and heavy machinery manufacturing.

This model thus serves as a valuable tool for industries seeking to enhance productivity, improve product consistency, and reduce costs in sinter forging operations.

V. Conclusion

The densification behavior of sintered billets under deformation was analyzed considering varying aspect ratios and initial relative densities under dynamic conditions using the modified upper bound method. The following conclusions can be drawn:

• Low-density billets achieve rapid densification with increasing percentage height reduction compared to high-density preforms. This is attributed to their higher initial porosity, which allows faster compaction during the early stages of deformation.

• High-aspect-ratio billets densify more quickly than low-aspect-ratio billets. The geometry of high-aspect-ratio billets facilitates better material flow and enhances compaction efficiency during the deformation process.

• The densification rate is not uniform for all billets. The aspect ratio and initial relative density significantly influence the compaction dynamics. High-aspect-ratio and low-initial-density billets exhibit faster densification due to their inherent geometrical and material properties. The modeling approach successfully predicted the pressure and densification characteristics by incorporating critical dynamic factors such as height reduction, billet expansion, sticking radius, and friction. The predictions align closely with experimental observations, highlighting the reliability and industrial applicability of the model.

Overall, the study demonstrates that understanding the influence of aspect ratio and relative density is crucial for optimizing the sinter forging process. The model is also able to predict the final product geometry aspect ratio. These insights can guide the design and processing of sintered components for improved mechanical performance and manufacturing efficiency. The proposed upper-bound method not only improves the accuracy of pressure estimation in sinter forging but also significantly reduces computational costs. This makes it a viable alternative to traditional methods like finite element analysis (FEA), especially for industries focused on high-volume production. By reducing the need for extensive trial-and-error experiments and energy-intensive simulations, this approach promotes sustainability by optimizing material and energy usage. The integration of this model into industrial software aligns with the principles of Industry 4.0, where predictive analytics

and digital twins play a pivotal role in optimizing processes. By digitizing the sinter forging process, the model supports the shift toward intelligent, data-driven manufacturing systems.

VI. Acknowledgments

Navdeep's work is supported by the Council of Scientific and Industrial Research (CSIR), Govt. of India (Award no. 09/1256(15849)/2022-EMR-1). Dr. Parveen Kumar expresses his gratitude for the financial support from the Department of Science & Technology, New Delhi, India, for Purse (SR/PURSE/2022/126).

Nomenclature

- μ_0: Constant dependent on lubricant.
- ρ_i: Density at the current height reduction point.
- ϵ: Constant exponent modulating the density dependence of μ.
- ρ_f: Final density.
- ρ_i: Initial density at the i_{th} height reduction step.
- ν: Poisson's ratio.
- Δh: Reduction in height.
- h: Initial height.
- b: Initial width of the preform.
- r_m: Sticking radius.
- ρ_p: Powder density.
- σ_0: Stress of the solid material.
- η: Strain-hardening factor.
- h: Instantaneous thickness of the workpiece.
- n: Constant quantity much greater than unity.
- p: Pressure at the die-workpiece interface.
- P: Die load and r, θ, z: Cylindrical coordinates.
- U: Die velocity, $\dot{U}$: Acceleration and U_i: Displacement rate field.
- ΔV: Magnitude of the relative velocity and b: Radius of the disc.
- ε: Strain and $\dot{\varepsilon}_{ij}$: Corresponding strain rate tensor field.
- η: Constant, a function of relative density ρ.
- λ: Flow stress of the sintered material and τ: Shear stress.
- μ: Coefficient of friction and a_i: Associated acceleration field.
- σ_0: Yield stress of the non-work-hardening matrix metal.
- ϕ_0: Specific cohesion of the contact surface.

Conflict of interest

The author declares no conflicts of interest in this paper.

References

I. Agrawal M., Jha A. K., Kumar S., "High-speed forging of hollow metal powder preforms", Inst. Engrs. (I) J., 80 (1999),8.

II. Avitzur B., "Metal Forming Processes and Analysis", McGraw Hill, New York, 1968.

III. Cost savings win the day for PM parts, Metal Powder Report, Vol. 56, Issue 7-8, (2001), 10-14.

IV. Jain Shrikant, Ranjan R. K. and Kumar Surender, "Fracturing and Deformation Characteristics of Aluminium Preform during Cold Forging at Low Strain Rates". Int. J. of Scientific Engineering and Technology, 4(3) (2015),182-186. 10.17950/ijset/v4s3/314

V. Jha A. K and Kumar S., "Analysis of Axisymmetric Cold Processing of Metal Powder Preforms", Journal of the Institution of Engineers (India), 65, (1985), 169.

VI. Jha A.K., Kumar S., "Dynamic effects during a high-speed sinter-forging process", International Journal of Machine Tools and Manufacture, Vol. 36, Issue 10, (1996), 1109-1122, ISSN 0890-6955. 10.1016/0890-6955(95)00122-0

VII. Jha A. K., Kumar S., "Investigations into the high-speed forging of sintered copper powder strips", Journal of Materials Processing Technology,71(3), (1997), 394-401. 10.1016/S0924-0136(97)00104-0

VIII. Jha A. K., Kumar S., "Compatibility of sintered materials during cold forging", International Journal of Materials and Product Technology' 9, Issue 4-6, (2004), 281-299. 10.1504/IJMPT.1994.036423

IX. Jones P. K., "The technical and economic advantage of powder forged products", Powder Metallurgy, Vol. 13, Issue 26, (1970), 114-129.

X. Kumar Parveen, Ranjan R. K., Kumar Rajive, **"**Mechanics of deformation during open die forging of sintered preform: Comparative study by equilibrium and upper bound methods", ARPN Journal of Engineering and Applied Sciences, 6(6), (2011),83–93. https://arpnjournals.com/jeas/research_papers/rp_2011/jeas_0611_515.pdf

XI. Kumar Parveen, Ranjan R. K., Kumar Rajive, "Investigations of an axisymmetric compound flow behavior of sintered preform: An upper bound approach", International Journal of Pure and Applied Mathematics, Vol. 81, Issue 5, (2012), 671-691. https://www.ijpam.eu/contents/2012-81-5/2/2.pdf

XII. Kumar Parveen, Ranjan R. K., Kumar Rajive, "Mathematical modelling of forging of sintered preform: Comparative study of open and closed die", International Journal of Pure and Applied Mathematics, Vol. 82, Issue 2, (2012), 179-188. https://www.ijpam.eu/contents/2013-82-2/2/2.pdf

XIII. Singh S., Jha A. K., "Sintered preforms adds better value to aerospace components", Journal of Aerospace Engineering, I. E. (I), 82, (2001), 1-6.

XIV. Singh Saranjit, Jha A.K., "Analysis of dynamic effects during high-speed forging of sintered preforms", Journal of Materials Processing Technology, Volume 112, Issue 1, 2001, Pages 53-62, ISSN 0924-0136 10.1016/S0924-0136(00)00898-0

XV. Singh S., Jha A. K., "An energy analysis during forging of sintered truncated conical preform at high-speed", Tamkang J. of Science and Engineering,7,(2004),227-236. http://jase.tku.edu.tw/articles/jase-200412-7-4-05

XVI. Singh Saranjit & Jha A. K. & Kumar Suhas. "Dynamic effects during sinter forging of axi-symmetric hollow disc preforms", International Journal of Machine Tools and Manufacture, Vol. 47, Issue 7-8,(2007),1101-1113. 10.1016/J.IJMACHTOOLS.2006.09.023

XVII. Tabata T., Masaki S. and Abe Y., "Analysis of Forging P/M Preforms" Journal of the Japan Society for Technology of Plasticity, 18, (1977), 373.

XVIII. Tabata T., Masaki S. and Hosokawa K., "A Compression Test to Determine the Coefficient of Friction in Forging P/M Preforms", International Journal of Powder Metallurgy Powder Technology, 16, (1980), 149.